Plasmonic-Enhanced Molecular Fluorescence within Isolated Bowtie Nano-Apertures

Guowei Lu, Wenqiang Li, Tianyue Zhang, Song Yue, Jie Liu, Lei Hou, Zhi Li, and Qihuang Gong*

State Key Laboratory for Mesoscopic Physics and Department of Physics, Peking University, Beijing 100871, China.

ABSTRACT

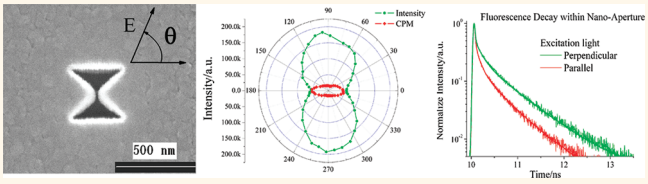

We report experimental behaviors of polarization-dependent, plasmonic-enhanced molecular fluorescence within isolated bowtie nano-apertures (BNAs) milled in aluminum films. BNAs provide efficient control of the fluorescent count rate per molecule and the decay lifetime of the molecules and provide an effective detection volume at the nanometer scale by tuning either the excitation light polarization or the BNA size. Interestingly, large BNAs (>300 nm) present high plasmonic-enhanced fluorescence efficiency and can simultaneously confine the detection volume below the subdiffraction limit. Numerical simulations were performed that agreed qualitatively with the experimental results. The BNAs have potential applications, especially for single-molecule biological analysis.

KEYWORDS: fluorescence · bowtie nano-aperture · plasmonic · lifetime · scattering

The highly efficient capability to confine light within a nanoscale volume is of great interest in the study of light interaction with biological materials and nanostructures,[1,2] in particular, for the efficient detection of the (generally weak) fluorescence signals emitted by an individual molecule or quantum dot. To overcome the detection limits set by optical diffraction, the environment surrounding an emitter can be tailored to control the local excitation intensity, quantum yield efficiency, and the angular radiation pattern.[3−6] Plasmonic nanostructure antennas create highly enhanced local fields when pumped resonantly, resulting in a greatly enhanced absorption or excitation of emitters,[7,8] leading to increased spontaneous fluorescence emission. The plasmonic antennas also allow nanoscale control of the lifetime,[9−12] spectra,[13−15] and direction[16−18] of photon emissions. Many groups have already reported fluorescent emission enhancement from emitters located in the vicinity of different types of metallic nanostructures: metallic nanoparticles,[7,12,14] core−shell particles,[11] nanoporous gold,[19] hole arrays and metallic gratings,[8,20,21] and single nano-apertures.[18,22−25]

Here, we have focused on isolated nano-apertures because, unlike regular nanoantennas, they are capable of blocking unwanted fluorescence signals by taking advantage of an opaque metal screen. In spite of their conceptual simplicity, these exhibit complex and interesting optical properties. For instance, metal-clad subwavelength circular apertures (also called "zero-mode waveguides") have been applied successfully in single-molecule analysis at high concentration and in real-time DNA sequencing.[22,26] Such nano-apertures exhibit a cutoff wavelength, above which no propagating modes exist inside the waveguide, the excitation field is evanescent coupling, and the intensity decays exponentially along the length, z, of the nano-aperture. The optimal diameter of aluminum circular nano-apertures for plasmonic-enhanced fluorescence excited at wavelength λ = 633 nm were elaborately investigated and found at ∼170 nm by Gerard *et al.*[23,27] The maximum fluorescence enhancement (∼7-fold) was related to the maximum density of photonic modes and to the minimum group velocity for the nonpropagative guided mode inside the circular nano-apertures. Furthermore, the propagative modes or nonpropagative evanescent modes were able to be tuned with good flexibility in rectangular nano-apertures by adjusting the excitation light polarization. The fluorescence intensity is enhanced significantly (∼ 3.2-fold) by the nonpropagative evanescent near-field within the rectangular nano-apertures, but there

* Address correspondence to qhgong@pku.edu.cn.

Received for review November 2, 2011 and accepted January 16, 2012.

Published online January 16, 2012
10.1021/nn2042412

is no obvious enhancement by propagative high-transmission modes.[25] The question arises for isolated nano-apertures milled in metallic thin films: can we expect a proper nanostructure with an increase in the fluorescence enhancement factor? To address this question, isolated bowtie nano-apertures (BNAs) were fabricated, enabling the fluorescence characteristics to be investigated in detail. To the best of our knowledge, the experimental investigation of plasmonic-enhanced molecular fluorescence within isolated BNAs has not been reported previously.

The optical properties of BNAs, such as the counterpart of the regular bowtie antennas as shown in Figure 1, have already been studied experimentally and theoretically by Xu *et al.*[28−30] In contrast to circular, rectangular, or square nano-apertures of the same opening area, BNAs have great potential to concentrate light within a superconfined spot with an intense local field. The coupling of induced electric fields at the tips of both arms with the propagative waveguide mode mainly confines the transmitted light within the nanoscale gap region. Enhanced light transmission through BNAs has been applied successfully in high-resolution nanoscale lithographic fabrication and high-throughput near-field optical probes.[30−33] BNAs provide not only an intense localized excitation field able to generate a high fluorescence enhancement factor but also an asymmetric structure for a tunable, polarization-dependent, plasmonic-enhanced excitation. In this study, the plasmonic-enhanced molecular fluorescence within isolated BNAs was studied by fluorescence correlation spectroscopy and lifetime measurements based on time-correlated single photon counting in an aqueous solution. The fluorescent behaviors are novel and clearly different from those within circular or rectangular nano-apertures. With an appropriate polarized excitation light, the fluorescence rate per molecule is significantly enhanced (~12-fold) within BNAs and the fluorescence lifetime and excitation volume are tunable by the excitation light polarization. Large BNAs (>300 nm) rather than small ones were found to enhance fluorescence more efficiently and could simultaneously confine the detection volume below the subdiffraction limit. These results are highly relevant to the strong interest in understanding the interactions between emitters and plasmonic antenna.

RESULTS AND DISCUSSION

The BNAs used in this study were fabricated by direct-focused ion beam (FIB) milling in ~170 nm thick aluminum films that were thermally evaporated on glass coverslip substrates. The angle of the bowtie's arms indicated in Figure 1a was fixed at ~90°, and the BNA gap (*i.e.*, the separation between the two arms) was fixed at ~30 nm, whereas the outline dimensions of the BNAs were tunable from 150 to 450 nm to

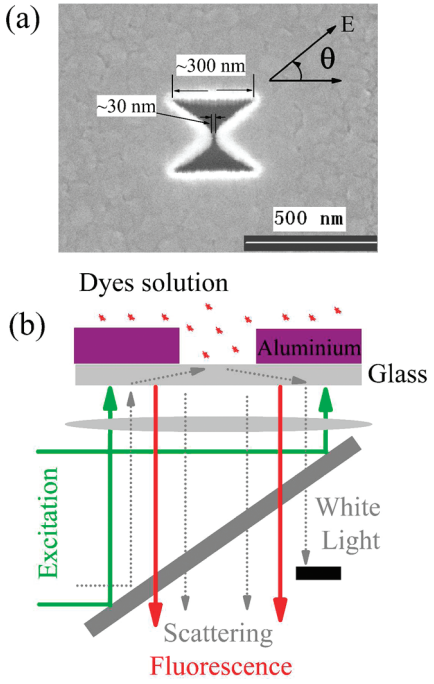

Figure 1. (a) Scanning electron microscope (SEM) image of a BNA with a ~300 nm outline size milled into a 170 nm thick aluminum thin film. (b) Schematic view of experimental optical configuration for fluorescence correlation spectroscopy, fluorescence decay lifetime, and white light total internal reflection scattering spectra measurements.

investigate how BNA size affected the molecular fluorescence within them. Initially, to gain insight into possible plasmonic resonances at specific wavelengths, the scattering spectrum of single isolated BNAs was measured using white light total internal reflection method based on a high numerical aperture objective lens.[34,35] Full instrumental details, including an instrument schematic, can be found in the Supporting Information. Typical scattering spectra of the isolated BNAs are shown in Figure 2a for different outline sizes illuminated by nonpolarized total internal reflection white light. As can be seen, there are clear characteristic resonance peaks at a wavelength of ~650 nm in the scattering spectra. The scattering spectra peaks were red-shifted with increasing BNA size, except for the 450 nm BNA. These results are in agreement with previous experimental transmittance spectra reported by Wang *et al.*,[29] where a wavelength tunable laser source was used to measure the transmission spectrum. In addition, the trend in BNA scattering variation is similar to that for isolated circular nano-apertures, which also display size dependence in surface plasmon resonance.[36,37]

To understand well the characteristic scattering spectra of the BNAs, the finite-difference time-domain (FDTD) method[38−40] was employed to calculate the absorption spectrum. Normal incident illumination light polarizes parallel to the BNA axis (*i.e.*, $\theta = 0°$) during FDTD simulation. As seen in Figure 2b, the

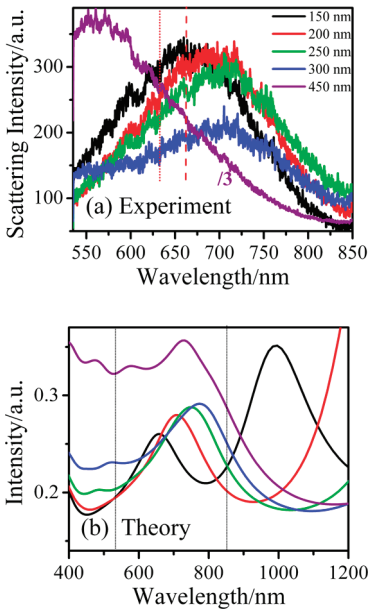

Figure 2. (a) Experimental white light total internal reflection scattering spectra for BNAs with various outline sizes, as indicated in the figure. (b) Simulation absorption spectra for the BNAs as above calculated by the FDTD method. The gray lines in (b) specify the spectrum range during experimental measurements.

numerical simulations agreed qualitatively with the experimental results. The calculated absorption spectra present two notable plasmonic resonance peaks in the visible and near-infrared range, and the spectral peak maximum red-shifted with increasing BNA outline size. The characteristic bands could be ascribed to the hybridization plasmonic mode, that is, the bonding and antibonding mode of the BNA's two arms.[41,42] The scattering spectral peaks observed experimentally at $\lambda \sim 650$ nm could be attributed to the antibonding mode, but the peak in the infrared range was not detectable because of the limit in the optical setup. To the best of our knowledge, this is the first report of such white light response properties of BNAs. These could be applied as plasmonic sensors by taking advantage of the high light concentration within the BNA gap,[36,37,43] but this is beyond the scope of this study. Additionally, there are unavoidable deviations between the theory and experiment. The most probable reasons of the theoretical results deviating from the experimental ones are (1) the BNA size deviations such as outline dimension size and gap separation adopted in the simulation deviating from the experimental ones, (2) the oblique internal wall and rough surface due to the intrinsic limit of FIB milling method which is not considered during the FDTD simulation, (3) aluminum material optical constant obtained from bulk material and fitted by the Drude–Lorentz model which should result in some deviation from the real situation. Nevertheless, we think the numerical simulation results provide a good qualitative explanation for the experimental results.

The existence of plasmon resonance in the BNAs and its relation to BNA geometry are beyond doubt, but more effort is required to fully understand the scattering spectra. Here, we focus our attention on the molecular fluorescence behaviors within the BNAs. As is well-known, extensive research has been reported on the optimization of fluorescence emission through matching the surface plasmon resonance with the excitation or emission bands of fluorescence molecules.[6−9] As indicated in Figure 2a, the excitation light (HeNe laser, $\lambda = 632.8$ nm) and collection emission band (Alex Fluor 647 dye molecules' emission filtered by a band-pass filter center, $\lambda = 660$ nm) are both within the plasmonic resonance band of the BNAs. This would result in plasmonic-enhanced molecular fluorescence within the BNAs.

Molecular Fluorescence within 450 nm BNAs. Molecular fluorescence within isolated BNAs was investigated by fluorescence correlation spectroscopy (FCS).[44,45] In the FCS method, the temporal fluctuations of the fluorescence signal, $I(t)$, are recorded and the temporal correlation of this signal is computed as $G(\tau) = \langle I(t) \times I(t+\tau)\rangle / \langle I(t)\rangle^2$, where τ is the delay (lag) time, and $\langle\ \rangle$ denotes time averaging. The amplitude of the correlation function quantifies the average number of molecules, N, and provides access to the fluorescence count rate per molecule, CPM $= (\langle I\rangle - \langle B\rangle)/N$, where $\langle B\rangle$ is the mean background noise. The incident excitation light is from below the sample (glass coverslip substrate), with linear polarization as shown schematically in Figure 1b. Unless otherwise stated, the excitation power of the HeNe laser was kept at 60 μW, measured before the entrance of the inverted optical microscope. For all experiments reported here, a solution of Alexa Fluor 647 molecules (A647, Invitrogen) at micromolar concentration ($\sim$2 μM) was deposited upon the surface of the thin film containing the nano-apertures. It should be pointed out that, because of the stochastic nature of the FCS technique, all of the measured fluorescence data here were temporally and spatially averaged over all of the possible molecular orientations and positions within the detection volume.

The polarization of excitation light was adjusted though a half-wavelength plate. Typical FCS results within the 450 nm BNA are shown in Figure 3a for excitation light polarizing parallel (*i.e.*, $\theta = 0°$) or perpendicular to the bowtie axis (*i.e.*, $\theta = 90°$), respectively. For comparison, FCS curves within the BNA (using $\sim$2 μM, as indicated above) and in the absence of nanostructures (using 5 nM dye solution as a free, open aqueous solution upon the bare glass coverslip) are normalized together in the Figure 3a inset. The characteristic diffusion time within the BNA was obviously shorter than that in free open solution, which implies a smaller effective detection volume because of the BNAs' confinement effect. Meanwhile, the $G_{(0)}$ values for the FCS curves within the BNAs increased

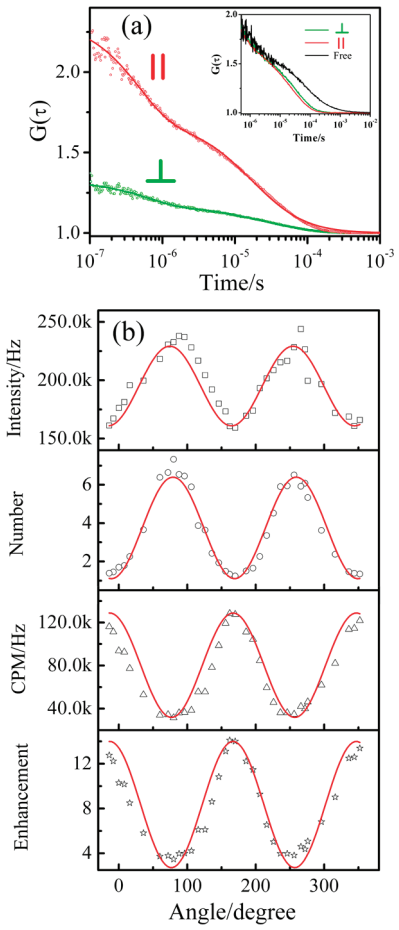

Figure 3. (a) Typical fluorescence correlation spectroscopy curves within a ~450 nm BNA for parallel (red) and perpendicular (green) polarization excitations. For comparison, the normalized FCS curves in free open solution and within the BNA are shown together. (b) Detected total fluorescence intensity, number of molecules within the detection volume, molecular CPM, and fluorescence CPM enhancement within the 450 nm nano-aperture as a function of the angle (*i.e.*, θ as indicated in Figure 1) between the illumination light polarization and the BNA gap axis. The solid lines are fitted curves according to the formula $a \cos^2 \theta + b$.

markedly compared with that of the free open solution (data not shown here), which is consistent with the conclusion drawn from the characteristic diffusion time. In addition, as shown in the Figure 3a inset, the diffusion time within the BNA under parallel excitation was shorter than that under perpendicular excitation, which means that the excitation field is obviously polarization-dependent. As seen in Figure 3a, the $G_{(0)}$ value under parallel excitation was significantly higher than that under perpendicular excitation, which confirms the smaller effective detection volume existing under parallel excitation. To gain more insight into this polarization-dependent phenomenon, the total fluorescent signal intensity, effective averaged molecule number, CPM, and fluorescence enhancement (*i.e.*, ratio of the CPM within BNA to that in free open solution) within the 450 nm BNA under different excitation polarization angles are summarized in

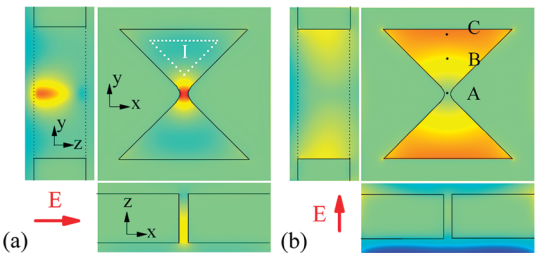

Figure 4. Electromagnetic field distributions calculated by the FDTD method for the 450 nm BNA by parallel (a) or perpendicular (b) polarization light propagating along the *z* direction. The field distributions are shown in *x*−*y*, *y*−*z*, and *x*−*z* plane sections crossing the BNA center.

Figure 3b. These values all show strong polarization dependence and can be fitted well with the formula $a \cos^2 \theta + b$, where θ is the angle between the light polarization and the bowtie axis. The CPM enhancements within the 450 nm BNA were ~3- and ~12-fold for perpendicular and parallel polarization illumination, respectively.

FDTD numerical simulations were performed to better understand the plasmonic-enhanced fluorescence with the BNAs. First, the electromagnetic field distributions within the 450 nm BNA were calculated for parallel or perpendicular polarization light illumination. Typical simulation results are shown in Figure 4 for three cross section planes at the BNA center. For convenience, the area enclosed by the white dotted line in Figure 4a, where it is relatively far from the metal surface, is called "region I". For parallel illumination light, the field intensity enhancement was about 5-fold at the center of the BNA gap, and in contrast, the field intensity decreased in region I. This means that the propagative transmission electromagnetic field is mainly confined and enhanced near the BNA gap. For perpendicular light, the light field intensity within the BNA gap was very weak but was reduced only slightly in region I. As shown in Figure 4b, the light was confined near the parallel edges of the BNA, similar to triangular nano-apertures.[46] Experimental measurements by scanning near-field optical microscope directly demonstrated such polarization dependence of the field distribution near BNAs.[47]

Thus, for parallel illumination light, the excitation volume is confined and enhanced around the BNA gap, which results in a smaller excitation volume, a higher $G_{(0)}$ value and a larger CPM than that by perpendicular light. On the other hand, the total fluorescence signal under perpendicular light illumination is higher. This can be understood as follows: although the light field intensity enhancement and molecular CPM is much lower near the BNA gap under perpendicular light, the field intensity and CPM in region I are much larger than that under parallel light illumination, and the volume of region I is much larger than the BNA gap volume. Thus, more molecules contribute to the total fluorescence

signal, which results in a higher total fluorescence signal count under perpendicular light illumination, as shown Figure 3b, even though the molecule CPM is low in region I. This is an interesting result, which contradicts that in rectangular nano-apertures, where the propagative transmission mode does not produce any fluorescence enhancement.[25] However, with the assistance of bowtie arms within the BNAs, the light is harvested around the BNA gap, resulting in a smaller excitation volume and high light density, which enhances the molecular fluorescence efficiently compared to the nonpropagative near-field mode.

Because the acquisition time of a FCS measurement is 30−120 s, it is believed that the concentration or distribution of the fluorescence molecules within the BNAs should be constant, irrespective of the excitation light polarization. (It should be pointed out that the optical trapping effect is neglected because of the low light intensity.) Thus, the observed strong polarization dependence phenomena are related to the local electromagnetic field distribution, assisted by the BNAs' surface plasmon resonance mode. As pointed out by Guo *et al.*,[47] the propagative transmission or nonpropagative near-field mode within BNAs is tunable by adjusting the light polarization, which is similar to rectangular nano-apertures. When the excitation light polarization is perpendicular to the BNA axis, the excitation light is a nonpropagative evanescent near-field, which is mainly confined within the BNA. In contrast, when the excitation light is parallel polarization light, the coupling between the propagative mode and the BNA gap structure results in a high transmission efficiency and a subwavelength confined spot.[28,30,47] As can be seen in Figure 3, the experimental results show that there was a smaller effective detection volume, higher CPM enhancement, and therefore a better signal/noise ratio by parallel excitation. In previous reports, the nonpropagative evanescent mode was the most effective for plasmonic-enhanced fluorescence within circular and rectangular nano-apertures.[22,23,25,48] In contrast, the novel propagative transmission mode within BNAs presents superior plasmonic-enhanced fluorescence performance than the nonpropagative evanescent mode. Also, the fluorescence enhancement within 450 nm BNAs was higher than that in circular or rectangular nano-apertures milled in aluminum thin films reported in the literature.[23,25,27] It should be pointed out that the fluorescence enhancements achieved by different research groups are not strictly comparable because the results are not acquired from the same individual chip. Nevertheless, the plasmonic-enhanced fluorescence within BNAs certainly presents an interesting phenomenon and has the same potential applications as circular nano-apertures.

To better reveal the fluorescence behaviors within the BNAs, the fluorescence lifetimes were measured

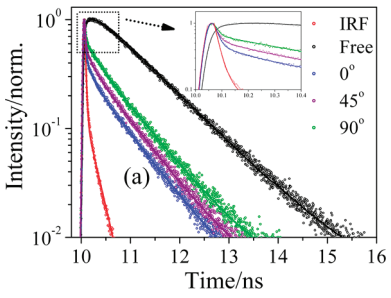

Figure 5. (a) Typical normalized fluorescence decay traces measured in a 450 nm BNA (blue for excitation polarization $\theta = 0°$, purple for $\theta = 45°$, and green for $\theta = 90°$). Dots are experimental data, and lines are numerical fitting lines. The shorter decay trace (red) is the overall instrument response function (IRF). The normalized fluorescence decay traces measured in free open solution are shown in black for comparison.

under various excitation polarizations. The molecule fluorescent decay lifetime in free open solution was about 0.98 ns, which corresponds well to the data in the literature.[48] Typical molecule fluorescence decay curves within 450 nm BNA are shown in Figure 5. The fluorescence molecular excitation state decay within the BNAs displayed two clear exponential features, regardless of the excitation polarization, both of which were shorter than that in free open solution. Here, the slow and fast decay components are referred to individually as τ_1 and τ_2. These components had values of 0.718 (±0.028) and 0.108 (±0.015) ns for parallel light excitation within the 450 nm BNAs and 0.783 (±0.012) and 0.171 (±0.006) ns for the perpendicular light excitation, respectively. This differs from the decay lifetimes in free open solution and circular or rectangular nano-apertures that display only monoexponential processes.[18,48] To verify our lifetime measurements, the fluorescence lifetimes within circular nano-apertures were also measured and found to display only a monoexponential process, as reported in the literature (the results for a ∼ 220 nm diameter circular nano-aperture are presented for comparison in the Supporting Information). The multiple processes of the fluorescence lifetime decay within the BNAs are probably related to the BNAs' high asymmetry compared to the circular or rectangular nano-apertures. The long lifetime τ_1 is attributed to the fluorescence signal from region I, where the coupling effect between the molecules and metal is weak because of large separations. The short lifetime τ_2 arises from the molecules locating around the BNA gap and parallel edges, due to the strong coupling effect between the molecules and metal. These results are supported by the numerical simulations by the FDTD method.

As is well-known, the spontaneous decay rate and quantum efficiency of an emitter can be drastically modulated by placing it in the vicinity of a plasmonic nanostructure.[3,4,49−51] The molecules within the BNAs present different decay rates and quantum yields

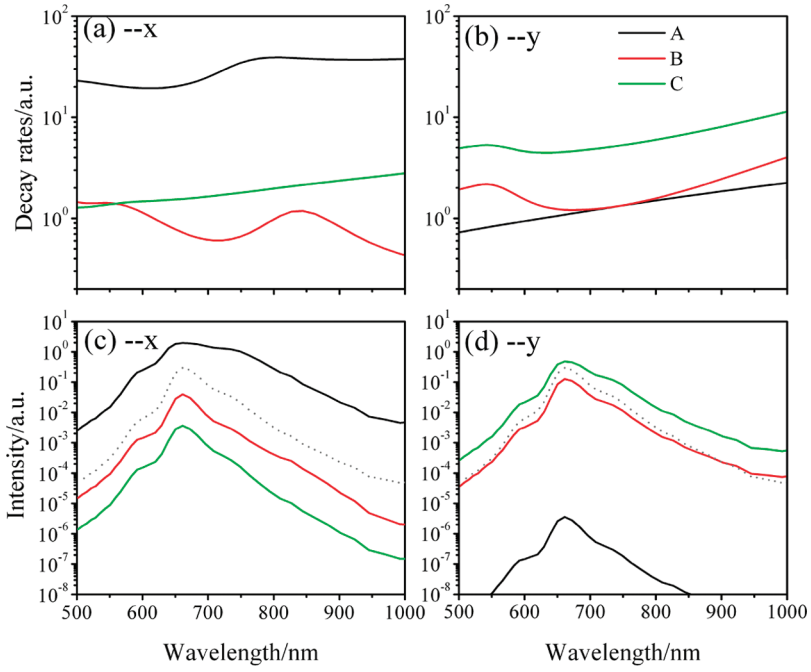

Figure 6. Normalized decay rates (top) and relative fluorescence enhancement (bottom) for points A (black), B (red), and C (green) with a 450 nm BNA, as indicated in Figure 4b. The left pictures are for the dipole parallel orientation along the BNA gap axis, and the right pictures are for the perpendicular dipole. The original fluorescence emission in gray is also plotted for comparison.

because of their different positions and orientations with respect to the BNAs. Here, the spontaneous molecular emissions within the BNAs were calculated by the FDTD method. Three typical points, as indicated in Figure 4b, are compared, that is, point A at the center of the BNA gap, point B located in the middle between the BNA gap center and parallel edge, and a separation between point C and the parallel edge of 15 nm. As seen in Figure 6a,b for the parallel oriented emitters (along the *x* direction), the normalized total decay rate of point A was the highest. On the contrary, for the perpendicular oriented emitters, point C was higher. The value at point B (belonging to region I) was always low, irrespective of orientation. These simulation results are in qualitative agreement with the above experimental results and offer a plausible explanation for the two distinct decay components seen in the lifetime measurements.

Additionally, the quantities of lifetime measurements in the BNAs are polarization-dependent. In previous reports,[9−12] molecules were fixed in a solid matrix, resulting in a fixed dipole orientation, giving a constant lifetime decay, regardless of the excitation light polarization. In contrast, here the molecules are free to diffuse in aqueous solution, so the molecules rotate freely in all directions. The measured lifetimes should therefore be an ergodic ensemble-averaged value during a typical 30−120 s measurement. As is well-known, molecules orientating in the direction of the excitation light polarization should be more effectively excited. Thus, the main excitation direction here is tuned by a linear polarized excitation light. For instance, when the excitation polarization aligns parallel to the BNAs axis, the molecules orientating along the BNA axis should be excited most efficiently. Meanwhile, the parallel oriented molecules within the BNA gap would more strongly couple with the BNA than those in a perpendicular orientation. Thus, the experimental results show that the decay lifetime is polarization-dependent. When the excitation light has perpendicular polarization, the molecules around the edge dominate the detected fluorescence signal for the faster decay process τ_2. On the other hand, for parallel light, the fluorescence signal for τ_2 is mainly from the BNA gap where the coupling between the molecules and metal is stronger, thus the lifetime is shorter, as supported by above numerical simulations. In addition, the deviation of τ_2 between parallel or perpendicular light is larger than is the case for τ_1 because the signal for decay process τ_1 is mainly from region I. These experimental results demonstrate that plasmonic antennas anisotropically modulate the decay rate of the molecules.

The relative fluorescence intensity of the molecules at the three points was also calculated as compared to the free open environments, and typical results are shown in Figure 6c,d. Usually, the fluorescence enhancement is considered to be the product of the excitation and emission enhancement: $\eta = \eta_{exc} \times \eta_{qye}$, where $\eta_{exc} = |pE|^2/|pE_0|^2$, $\eta_{qye} = 1/[(1 - \eta_0)/F + \eta_0/\eta_a]$, where F is the radiative Purcell factor, η_0 is the original molecular quantum yield efficiency, and η_a is the

TABLE 1. Molecule Fluorescence Characteristics within Various Size BNAs

BNAs		~150 nm	~200 nm	~250 nm	~300 nm	~450 nm
I_{total} (kHz)	∥ [a]	$20.2_{2.2}$ [d]	$28.6_{6.2}$	$46.3_{6.4}$	$67.1_{15.3}$	$152.3_{18.6}$
	⊥ [b]	$16.4_{2.9}$	$47.6_{8.7}$	$136.2_{12.3}$	$184.5_{15.8}$	$229.2_{16.7}$
	ratio [c]	1.23	0.60	0.34	0.36	0.66
η_{CPM}	∥	$2.7_{0.4}$	$2.1_{0.4}$	$3.6_{0.5}$	$5.4_{0.7}$	$11.9_{2.7}$
	⊥	$5.6_{1.4}$	$2.9_{0.3}$	$2.0_{0.4}$	$1.5_{0.5}$	$4.0_{1.1}$
	ratio	0.48	0.70	1.67	3.54	3.27
V_{eff} (aL)	∥	$0.65_{0.09}$	$1.22_{0.10}$	$1.28_{0.18}$	$1.11_{0.13}$	$1.09_{0.17}$
	⊥	$0.28_{0.06}$	$1.45_{0.24}$	$6.60_{1.08}$	$7.86_{0.96}$	$6.17_{0.77}$
	ratio	2.32	0.84	0.19	0.14	0.18
τ_1 (ns)	∥	$0.308_{0.05}$ [e]	$0.467_{0.11}$	$0.563_{0.19}$	$0.605_{0.25}$	$0.718_{0.51}$
	⊥	$0.271_{0.06}$	$0.482_{0.12}$	$0.532_{0.20}$	$0.690_{0.33}$	$0.783_{0.54}$
τ_2 (ns)	∥	$0.035_{0.95}$	$0.067_{0.89}$	$0.091_{0.81}$	$0.093_{0.75}$	$0.108_{0.49}$
	⊥	$0.041_{0.94}$	$0.071_{0.88}$	$0.076_{0.80}$	$0.109_{0.67}$	$0.171_{0.46}$

[a] Parallel excitation. [b] Perpendicular excitation. [c] The ratio of the value by parallel excitation to that by perpendicular excitation. [d] Measurement deviations. [e] Relative proportion of fluorescence signal intensity.

antenna emission efficiency. Similar to the molecule decay rates, the molecule emission quantum yield is also related to its position and orientation with respect to the BNA. For instance, the molecular fluorescence at point A is enhanced significantly when it orients parallel to the BNA gap axis, but the fluorescence is suppressed strongly for the perpendicular orientation. Thus, a low fluorescence signal comes from the BNA gap when the excitation light polarization is perpendicular, but for parallel excitation, the molecules orientating along the *x* direction emit at high efficiency and dominate the fluorescence fast decay component. Also, the relative proportion for fluorescence signal intensity of the fast decay process τ_2 by parallel excitation increases as shown in Figure 5 and Table 1 because of the high fluorescence enhancement by comparison with that of perpendicular excitation. Here, the simulation performed with a single dipole point provides a qualitative understanding of the plasmonic-enhanced molecule fluorescence within the BNAs.

Additionally, the coupling between the molecules and plasmonic nanostructure also influences the emission direction and therefore the collection efficiency. Here, the molecular emission pattern in the BNAs was not found to present an obvious anisotropic distribution by direct EMCCD imaging, as shown in the Supporting Information Figure S5, because the individual nano-aperture has a weak beaming ability compared with the one assisted by periodic corrugations acting as a grating antenna.[18,52] Recently, a method developed by Wenger *et al.* enabled experimental quantification of the respective contributions of the excitation and emission gains in circular nano-aperture enhanced fluorescence through analyzing the evolution of the fluorescence enhancement *versus* the excitation power.[48] The emission gain contains both a radiative rate enhancement and a collection efficiency enhancement. The fluorescence CPM within the BNAs *versus* the excitation power was also measured and is shown in the Supporting Information Figure S6, along with analysis data summarized in Supporting Information Table S1. Clearly, the CPM under parallel excitation was higher than that under perpendicular excitation light, and the saturation power by parallel excitation was lower due to the light concentration and enhancement effects of the BNA gap. The two exponential decay processes in the lifetime measurements of the BNAs cause some limitations in the extraction of the enhancement of decay rates and excitation rate efficiently, and therefore, the weighted average values were used for total decay rate enhancements. The characterization of the fluorescence enhancement shows that (i) both excitation and emission gains contributed to the overall fluorescence enhancement and (ii) the enhancement by parallel excitation light was higher both in excitation and emission compared with that by perpendicular light. These experimental results are in qualitative agreement with the above numerical simulation results.

Molecular Fluorescence within Different Outline Sizes of BNAs. Having investigated the molecule fluorescence behaviors within the 450 nm BNA in detail, we became interested in how the BNA size affects fluorescence. To answer this question and identify the optimal BNA size for fluorescence enhancement, BNAs with outline dimension sizes varying from 150 to 450 nm were investigated under polarized excitation light as above. Here, several BNAs with the same size were measured to ensure the reproducibility of experiments. Typical results are summarized in Table 1 only for parallel and perpendicular polarization excitation. (1) The total fluorescent intensity within the BNAs decreased with decreasing BNA size, regardless of the excitation polarization, as shown in Table 1. The fluorescence intensity excited by the perpendicular polarization light was higher and but decreased faster than that by the parallel light, which resulted in the ratio reversal for the 150 nm BNAs. This phenomena differs from regular bowtie antenna, where the signal intensity excited by parallel excitation was always found to be higher than that by perpendicular excitation.[9,10] (2) The molecule CPM also presents a clear difference between the small and large size BNAs. For larger BNAs, a higher CPM was obtained by parallel excitation, but for smaller BNAs, efficient enhancement occurs with perpendicular light. The molecule CPM did not present obvious polarization dependence in 200−250 nm BNAs. (3) The fluorescence lifetime measurements were also performed for the different BNA sizes. The decay lifetime decreased with decreasing size, regardless of the excitation polarization, which is similar to the trend seen in circular nano-apetures.[41] In addition, the relative proportion of fluorescence signal intensity for the fast

decay process τ_2 increased with decreasing BNA size, while it decreased for the slow decay process τ_1.

To better understand these phenomena, the field distribution, the decay rates, and antenna efficiency of 150 nm BNA were calculated and are shown in the Supporting Information Figures S7 and S8 for comparison with 450 nm BNA. As the BNA size decreases, fewer molecules contribute to the fluorescence signal, due to the physical confinement effect, and this results in the total fluorescent intensity within the BNAs decreasing as the size decreases. The volume of region I and near edges reduces more rapidly by comparison with the volume around the BNA gap. Recalling the results in Figure 6, the molecules located within region I or near the edges contribute most of the fluorescence signal for perpendicular incident light. Thus, total fluorescence intensity excited by perpendicular incident light decreases rapidly and even results in the ratio reversal for the 150 nm BNAs shown in Table 1. This conclusion can find support in the lifetime measurements. The slow decay process is believed to occur within region I because of the large separation between the molecules and the metal, resulting in a smaller coupling effect. As the BNA size decreases, the average separation between the molecules and the metallic surface decreases correspondingly, which leads to a decreased lifetime. In addition, the relative intensity of the fluorescence signal for the slow decay process also decreased with decreasing BNA size, as shown in Table 1. The simulation results are in qualitative agreement with the experimental results, as shown in Figure S8. The decay rate of the molecules at the BNA gap center was higher for BNAs of smaller size. Also, the parallel oriented dipole presents a higher decay rate compared with the perpendicular orientation. All of this evidence seems to provide a plausible and consistent qualitative explanation for the variation in total fluorescence intensity and lifetime results as BNA size changes.

The high CPM is beneficial to statistical accuracy in the FCS method because the signal-to-noise ratio in FCS depends on the CPM but not on the total detected fluorescence. Here, the molecule CPM also presents a ratio reversal between small and large size BNAs, while the trend in CPM variation as a function of BNA size is not monotonous. For simplicity, the results of 150 and 450 nm BNAs were compared in detail to understand how BNA size affects the CPM. For parallel excitation light, the simulation shows that field enhancement at the 150 nm BNA gap center was slightly higher (~20%) than that at the 450 nm BNA gap center, and the antenna efficiency of the 450 nm BNA was higher (~60%) than that of the 150 nm BNA, as shown in Figure S8. Therefore, the final CPM of the 450 nm BNA illuminated by parallel polarized light was higher than that of the 150 nm BNA. For perpendicular excitation light, the fluorescence enhancement by the parallel edges and corners must be considered together for small size BNAs because this becomes comparable with that by the BNA gap. In particular, the fluorescence contribution from region I of the 150 nm BNAs reduced greatly, where it should possess a lower enhancement efficiency by comparison with areas such as the gap, corner, or near the edges. Thus, in turn, the CPM of 150 nm BNAs was higher than that of 450 nm BNAs when illuminated by perpendicular polarized light. The effective detection volume confined by the BNAs plays a role in determining the final CPM. As shown in Table 1, the CPM ratio between parallel and perpendicular light presents a clear reversal between the small and large BNAs. The effective detection volume by perpendicular light obviously reduced when the BNAs were less than ~200 nm, probably due to the strong confinement of smaller sized apertures, resulting in exponential decay of the evanescent light at the bottom, as shown in Figure S7. It should be pointed out that the transmission mode of nano-apertures could lead to excited molecules in open solution and collected emission. This transmission could be one of the reasons leading to CPM polarization reversal for 150 nm BNAs. Additionally, the molecular emission direction modulated by the BNA antenna will significantly influence the fluorescence counts. Thus, an appropriate size would benefit the concentration of excitation light and *vice versa*, which would also modulate the emission process. In addition, the emission properties collected parallel and perpendicular to the excitation polarization were also investigated. The preliminary results are summarized in the Supporting Information Figure S10, and the results show that coupling between emitters and BNA also modulates the emission polarization. All of these factors should be taken into account when seeking to fully understand the physical origins of the phenomena, but this is beyond the scope of this study.

The effective detection volume is another important factor related to practical applications, and the results are also calibrated and summarized in Table 1 for different BNA sizes. Interestingly, by controlling the excitation polarization, the effective detection volume is tunable. As we can see, the variations in the effective detection volume (for example, a 300 nm BNA) can be up to an order, simply by tuning the excitation light polarization. The effective volumes excited by parallel polarization light always comprise ~1 aL (attoliter: 10^{-18} liter) for the different BNA sizes, apart from the 150 nm BNA, which means that the BNA gap volume is almost constant even as the BNA outline size changes. In particular, the 450 nm BNAs not only confined the effective detection volume to below the optical diffraction limit but simultaneously provided a highly efficient fluorescence enhancement, resulting in an improved signal/noise ratio. Therefore, large BNAs offer advantages when special surface treatments are needed to anchor or immobilize biological molecules,

especially for biological objects with large volumes that would obstruct their entrance into small nano-apertures. These results indicate that the BNA is a potential platform, similar to that offered by circular nano-apertures for biological applications at high molecule concentration,[22−25,27,48] and that large BNAs present interesting performance. It should be noted that the fluorescence enhancement performance within BNAs can be optimized further by appropriate material and structure choice. For instance, gold thin films with a suitable adhesion layer instead of aluminum films, because of low optical loss and obvious plasmon resonance in the visible range of gold material, would present higher fluorescence enhancements, as verified by previous reports for circular nano-apertures.[27,53] Recently, circular nano-apertures with plasmonic corrugations were reported to modulate the emission direction and greatly enhance fluorescence.[18,52] Such a structure should also be effective for BNA plasmonic-enhanced fluorescence, as recent experiments have demonstrated that the addition of a grating structure around aluminum BNAs can enhance significantly far-field transmission through the apertures.[54,55] This work is currently being conducted.

CONCLUSIONS

In summary, molecule fluorescence behaviors within isolated BNAs were studied in detail using numerical and experimental methods. First, we showed that the scattering spectra of BNAs display obvious plasmonic resonance and are size-dependent. The characteristic resonances of the BNAs covered the excitation laser light and dye molecule emission wavelengths, which allowed not only a large plasmonic enhancement of the excitation field but also an enhanced fluorescence decay rate to enable brighter emission. Interestingly, the fluorescence intensity, molecule CPM, excitation field distribution (*i.e.*, effective detection volume), and fluorescence decay lifetime all presented polarization dependence. The experimental phenomena were able to be explained qualitatively with the help of the FDTD theoretical simulations. A clear experimental demonstration was given that plasmonic antennas can modulate the decay rate of molecules oriented along different directions with respect to the gap axis of the bowtie aperture antenna. In particular, BNAs with a 300−450 nm outline size were able to significantly confine the detection volume (3 order reduction compared with the conventional light diffraction limit) by controlling the excitation polarization. Such large BNAs not only greatly enhance the molecule CPM but would also be suitable for biological or physical manipulation because of their large and accessible open dimensions.

METHODS

White Light Scattering Spectrum. The scattering spectrum of white light total internal reflection method based on a high numerical aperture objective lens was constructed and verified in previous reports.[34,35] A scheme of the setup is shown in the Supporting Information Figure S3. In brief, on the basis of an inverted Olympus optical microscope, a collimated white light beam was approximately focused at the back focal plane of a numerical aperture 1.45, 60× TIRF oil-immersion objective lens (Olympus, Japan). The scattering spectrum was collected by the same objective and directed into a spectrometer (NT-MDT, Russia), as shown schematically in Figure 1b.

Fluorescence Correlation Spectroscopy and Fluorescence Lifetime Measurements. The fluorescence correlation spectroscopy method was described in detail in our previous paper,[45] and the full instrumental details, including an instrument schematic, can be found in the Supporting Information Figure S2. Time-correlated single-photon counting (TCSPC) methods are also shown schematically in Figure S2. A picosecond laser diode operating at wavelength 635 nm with a repeat rate of 60 MHz (A.L.G. GmbH, Germany) was used in conjunction with a fast avalanche photodiode (Micro Photon Devices by PicoQuant MPD-5CTC). The photodiode output was coupled to a fast TCSPC module (PicoHarp 300, PicoQuant).

FDTD. (1) For the calculation of the field distribution, the Yee cell size used in our calculation was set at $1 \times 1 \times 1$ nm^3. A CW plane light at wavelength 633 nm propagated through the BNA along the *z* direction, and the number of periods of the incident plane wave was set to 12 to guarantee calculation convergence. (2) For the calculation of the decay rate and antenna efficiency, a single emitter was simply implemented in the FDTD by having a classical point current source placed in proximity to the nanostructure. The antenna efficiency can be obtained by calculating the ratio of the time-averaged power radiated to the far-field and the total power dissipated by the dipole.[51] Here, a point dipole was placed at the nano-aperture gap center oriented along the *x* or *y* directional electronic component to mimic a molecule orientating to the *x* or *y* axis. (3) For the calculation of A647 molecule fluorescence enhancement, the spectra of A647 dye in free open solution was used as the original molecule emission spectra with a quantum yield efficiency of 30%. The excitation field distribution at 633 nm and antenna efficiency at the same point within the BNAs were considered to give the relative fluorescence with comparison to the free case.

Acknowledgment. This work was supported by the National Natural Science Foundation of China (Grant Nos. 61008026, 10821062, and 90921008) and the National Basic Research Program of China (Grant Nos. 2007CB307001 and 2009CB930504).

Supporting Information Available: Fabrications and SEM images for the BNAs with different outline sizes; experimental setups and analysis method descriptions; fluorescence lifetime decay for BNAs with different outline sizes; fluorescence images from the nano-apertures; fluorescence counts rate per molecule *versus* the excitation power within 300 and 450 nm BNAs; the electromagnetic field distribution, decay rates, and antenna efficiency comparisons of 150 and 450 nm BNAs by the FDTD method; FCS and lifetime results of circular nano-aperture with a diameter of ∼220 nm for comparison; emission polarization resolved measurements by linear polarized excitation in free open solution and within ∼300 nm BNA. This material is available free of charge *via* the Internet at http://pubs.acs.org.

REFERENCES AND NOTES

1. Schuller, J. A.; Barnard, E. S.; Cai, W.; Jun, Y. C.; White, J. S.; Brongersma, M. L. Plasmonics for Extreme Light Concentration and Manipulation. *Nat. Mater.* **2011**, *9*, 193–204.

2. Wang, F.; Shen, Y. R. General Properties of Local Plasmons in Metal Nanostructures. *Phys. Rev. Lett.* **2006**, *97*, 206806–206809.
3. Purcell, E. M. Spontaneous Emission Probabilities at Radio Frequencies. *Phys. Rev.* **1946**, *69*, 681.
4. Drexhage, K. H. Interaction of Light with Monomolecular Dye Layers. *Prog. Opt.* **1974**, *12*, 165.
5. Gerard, J. M.; Sermage, B.; Gayral, B.; Legrand, B.; Costard, E.; Thierry-Mieg, V. Enhanced Spontaneous Emission by Quantum Boxes in a Monolithic Optical Microcavity. *Phys. Rev. Lett.* **1998**, *81*, 1110–1113.
6. Emmanuel, F.; Samuel, G. Surface Enhanced Fluorescence. *J. Phys. D: Appl. Phys.* **2008**, *41*, 013001.
7. Anger, P.; Bharadwaj, P.; Novotny, L. Enhancement and Quenching of Single-Molecule Fluorescence. *Phys. Rev. Lett.* **2006**, *96*, 113002–113005.
8. Pompa, P. P.; Martiradonna, L.; Della Torre, A.; Della Sala, F.; Manna, L.; de Vittorio, M.; Calabi, F.; Cingolani, R.; Rinaldi, R. Metal-Enhanced Fluorescence of Colloidal Nanocrystals with Nanoscale Control. *Nat. Nanotechnol.* **2006**, *1*, 126–130.
9. Kinkhabwala, A.; Yu, Z.; Fan, S.; Avlasevich, Y.; Mullen, K.; Moerner, W. E. Large Single-Molecule Fluorescence Enhancements Produced by a Bowtie Nanoantenna. *Nat. Photonics* **2009**, *3*, 654–657.
10. Muskens, O. L.; Giannini, V.; Sanchez-Gil, J. A.; Gomez Rivas, J. Strong Enhancement of the Radiative Decay Rate of Emitters by Single Plasmonic Nanoantennas. *Nano Lett.* **2007**, *7*, 2871–2875.
11. Bardhan, R.; Grady, N. K.; Halas, N. J. Nanoscale Control of Near-Infrared Fluorescence Enhancement Using Au Nanoshells. *Small* **2008**, *4*, 1716–1722.
12. Kuhn, S.; Hakanson, U.; Rogobete, L.; Sandoghdar, V. Enhancement of Single-Molecule Fluorescence Using a Gold Nanoparticle as an Optical Nanoantenna. *Phys. Rev. Lett.* **2006**, *97*, 017402–017405.
13. Ming, T.; Zhao, L.; Yang, Z.; Chen, H.; Sun, L.; Wang, J.; Yan, C. Strong Polarization Dependence of Plasmon-Enhanced Fluorescence on Single Gold Nanorods. *Nano Lett.* **2009**, *9*, 3896–3903.
14. Ringler, M.; Schwemer, A.; Wunderlich, M.; Nichtl, A.; Kurzinger, K.; Klar, T. A.; Feldmann, J. Shaping Emission Spectra of Fluorescent Molecules with Single Plasmonic Nanoresonators. *Phys. Rev. Lett.* **2008**, *100*, 203002–203005.
15. Bakker, R. M.; Yuan, H.; Liu, Z.; Drachev, V. P.; Kildishev, A. V.; Shalaev, V. M.; Pedersen, R. H.; Gresillon, S.; Boltasseva, A. Enhanced Localized Fluorescence in Plasmonic Nanoantenna. *Appl. Phys. Lett.* **2008**, *92*, 043101–043103.
16. Gersen, H.; Garcia-Parajo, M. F.; Novotny, L.; Veerman, J. A.; Kuipers, L.; van Hulst, N. F. Influencing the Angular Emission of a Single Molecule. *Phys. Rev. Lett.* **2000**, *85*, 5312–5315.
17. Taminiau, T. H.; Stefani, F. D.; Segerink, F. B.; Van Hulst, N. F. Optical Antennas Direct Single-Molecule Emission. *Nat. Photonics* **2008**, *2*, 234–237.
18. Aouani, H.; Mahboub, O.; Devaux, E.; Rigneault, H.; Ebbesen, T. W.; Wenger, J. Plasmonic Antennas for Directional Sorting of Fluorescence Emission. *Nano Lett.* **2011**, *11*, 2400–2406.
19. Biteen, J. S.; Pacifici, D.; Lewis, N. S.; Atwater, H. A. Enhanced Radiative Emission Rate and Quantum Efficiency in Coupled Silicon Nanocrystal Nanostructured Gold Emitters. *Nano Lett.* **2005**, *5*, 1768–1773.
20. Liu, Y.; Blair, S. Fluorescence Enhancement from an Array of Subwavelength Metal Apertures. *Opt. Lett.* **2003**, *28*, 507–509.
21. Kim, J. H.; Moyer, P. J. Laser-Induced Fluorescence within Subwavelength Metallic Arrays of Nanoholes Indicating Minimal Dependence on Hole Periodicity. *Appl. Phys. Lett.* **2007**, *90*, 131111–131113.
22. Levene, M. J.; Korlach, J.; Turner, S. W.; Foquet, M.; Craighead, H. G.; Webb, W. W. Zero-Mode Waveguides for Single-Molecule Analysis at High Concentrations. *Science* **2003**, *299*, 682–686.
23. Rigneault, H.; Capoulade, J.; Dintinger, J.; Wenger, J.; Bonod, N.; Popov, E.; Ebbesen, T. W.; Lenne, P.-F. Enhancement of Single-Molecule Fluorescence Detection in Subwavelength Apertures. *Phys. Rev. Lett.* **2005**, *95*, 117401–117404.
24. Wenger, J.; Gerard, D.; Lenne, P.-F.; Rigneault, H.; Bonod, N.; Popov, E.; Marguet, D.; Nelep, C.; Ebbesen, T. W. Biophotonics Applications of Nanometric Apertures. *Int. J. Mater. Prod. Technol.* **2009**, *34*, 488–506.
25. Wenger, J.; Lenne, P.-F.; Popov, E.; Rigneault, H.; Dintinger, J.; Ebbesen, T. W. Single Molecule Fluorescence in Rectangular Nano-Apertures. *Opt. Express* **2005**, *13*, 7035–7044.
26. Eid, J.; Fehr, A.; Gray, J.; Luong, K.; Lyle, J.; Otto, G.; Peluso, P.; Rank, D.; Baybayan, P.; Bettman, B.; *et al.* Real-Time DNA Sequencing from Single Polymerase Molecules. *Science* **2009**, *323*, 133–138.
27. Gerard, D.; Wenger, J.; Bonod, N.; Popov, E.; Rigneault, H. Nanoaperture-Enhanced Fluorescence: Towards Higher Detection Rates with Plasmonic Metals. *Phys. Rev. B* **2008**, *77*, 045413–045419.
28. Jin, E. X.; Xu, X. Enhanced Optical Near Field from a Bowtie Aperture. *Appl. Phys. Lett.* **2006**, *88*, 153110–153112.
29. Wang, L.; Xu, X. Spectral Resonance of Nanoscale Bowtie Apertures in Visible Wavelength. *Appl. Phys. A: Mater. Sci. Process.* **2007**, *89*, 293–297.
30. Wang, L.; Uppuluri, S. M.; Jin, E. X.; Xu, X. Nanolithography Using High Transmission Nanoscale Bowtie Aperture. *Nano Lett.* **2006**, *6*, 361–364.
31. Sendur, K.; Challener, W. Near-Field Radiation of Bowtie Antennas and Apertures at Optical Frequencies. *J. Microsc.* **2002**, *210*, 279–283.
32. Mivelle, M.; Ibrahim, I. A.; Baida1, F.; Burr, G. W.; Nedeljkovic, D.; Charraut, D.; Rauch, J.-Y.; Salut, R.; Grosjean, T. Bowtie Nano-Aperture as Interface between Near-Fields and a Single-Mode Fiber. *Opt. Express* **2010**, *18*, 15964–15974.
33. Onuta, T. D.; Waegele, M.; DuFort, C. C.; Schaich, W. L.; Dragnea, B. Optical Field Enhancement at Cusps between Adjacent Nanoapertures. *Nano Lett.* **2007**, *7*, 557–564.
34. Kalkbrenner, T.; Hakanson, U.; Sandoghdar, V. Tomographic Plasmon Spectroscopy of a Single Gold Nanoparticle. *Nano Lett.* **2004**, *4*, 2309–2314.
35. Stiles, R. L.; Willets, K. A.; Sherry, L. J.; Roden, J. M.; Van Duyne, R. P. Investigating Tip−Nanoparticle Interactions in Spatially Correlated Total Internal Reflection Plasmon Spectroscopy and Atomic Force Microscopy. *J. Phys. Chem. C* **2008**, *112*, 11696–11701.
36. Rindzevicius, T.; Alaverdyan, Y.; Dahlin, A.; Hook, F.; Sutherland, D. S.; Kall, M. Plasmonic Sensing Characteristics of Single Nanometric Holes. *Nano Lett.* **2005**, *5*, 2335–2339.
37. Prikulis, J.; Hanarp, P.; Olofsson, L.; Sutherland, D.; Käll, M. Optical Spectroscopy of Nanometric Holes in Thin Gold Films. *Nano Lett.* **2004**, *4*, 1003–1007.
38. Taflove, A.; Hagness, S. C. Computational Electrodynamics: *The Finite-Di□erence Time-Domain Method*, 3rd ed.; Artech House: Norwood, MA, 2005.
39. Oskooi, A. F.; Roundy, D.; Ibanescu, M.; Bermel, P.; Joannopoulos, J. D.; Johnson, S. G. Meep: A Flexible Free-Software Package for Electromagnetic Simulations by the FDTD Method. *Comput. Phys. Commun.* **2010**, *181*, 687–702.
40. Kaminski, F.; Sandoghdar, V.; Agio, M. Finite-Difference Time-Domain Modeling of Decay Rates in the Near Field of Metal Nanostructures. *J. Comput. Theor. Nanosci.* **2007**, *4*, 635–643.
41. Nordlander, P.; Oubre, C.; Prodan, E.; Li, K.; Stockman, M. I. Plasmon Hybridization in Nanoparticle Dimers. *Nano Lett.* **2004**, *4*, 899–903.
42. Funston, A. M.; Novo, C.; Davis, T. J.; Mulvaney, P. Plasmon Coupling of Gold Nanorods at Short Distances and in Different Geometries. *Nano Lett.* **2009**, *9*, 1651–1658.
43. Feuz, L.; Jonsson, P.; Jonsson, M. P.; Hook, F. Improving the Limit of Detection of Nanoscale Sensors by Directed Binding to High-Sensitivity Areas. *ACS Nano* **2010**, *4*, 2167–2177.
44. Lu, G.; Lei, H. F.; Angiboust, J. F.; Manfait, M. Confined Detection Volume of Fluorescence Correlation Spectroscopy by Bare Fiber Probes. *Eur. Biophys. J.* **2010**, *39*, 855–860.

45. Wang, Q.; Lu, G.; Hou, L.; Zhang, T.; Luo, C.; Yang, H.; Barbillon, G.; Lei, H. F.; Marquette, C. A.; Perriat, P.; *et al.* Fluorescence Correlation Spectroscopy near Individual Gold Nanoparticle. *Chem. Phys. Lett.* **2011**, *503*, 256–261.
46. Naber, A.; Molenda, D.; Fischer, U. C.; Maas, H.-J.; Hoppener, C.; Lu, N.; Fuchs, H. Enhanced Light Confinement in a Near-Field Optical Probe with a Triangular Aperture. *Phys. Rev. Lett.* **2002**, *89*, 210801–210801.
47. Guo, R.; Kinzel, E. C.; Li, Y.; Uppuluri, S. M.; Raman, A.; Xu, X. Three-Dimensional Mapping of Optical Near Field of a Nanoscale Bowtie Antenna. *Opt. Express* **2010**, *18*, 4961–4971.
48. Wenger, J.; Gerard, D.; Bonod, N.; Popov, E.; Rigneault, H.; Dintinger, J.; Mahboub, O.; Ebbesen, T. W. Emission and Excitation Contributions to Enhanced Single Molecule Fluorescence by Gold Nanometric Apertures. *Opt. Express* **2008**, *16*, 3008–3020.
49. Enderlein, J. Theoretical Study of Single Molecule Fluorescence in a Metallic Nanocavity. *Appl. Phys. Lett.* **2002**, *80*, 315–317.
50. Lu, G.; Zhang, T.; Li, W.; Hou, L.; Liu, J.; Gong, Q. Single-Molecule Spontaneous Emission in the Vicinity of an Individual Gold Nanorod. *J. Phys. Chem. C* **2011**, *115*, 15822–15828.
51. Liaw, J.; Chen, J.; Chen, C.; Kuo, M. Purcell Effect of Nanoshell Dimer on Single Molecule's Fluorescence. *Opt. Express* **2009**, *17*, 13532–13540.
52. Aouani, H.; Mahboub, O.; Bonod, N.; Devaux, E.; Popov, E.; Rigneault, H.; Ebbesen, T. W.; Wenger, J. Bright Unidirectional Fluorescence Emission of Molecules in a Nanoaperture with Plasmonic Corrugations. *Nano Lett.* **2011**, *11*, 637–644.
53. Aouani, H.; Wenger, J.; Gérard, D.; Rigneault, H.; Devaux, E.; Ebbesen, T. W.; Mahdavi, F.; Xu, T.; Blair, S. Crucial Role of the Adhesion Layer on the Plasmonic Fluorescence Enhancement. *ACS Nano* **2009**, *3*, 2043–2048.
54. Kinzel, E. C.; Srisungsitthisunti, P.; Li, Y.; Raman, A.; Xu, X. Extraordinary Transmission from High-Gain Nanoaperture Antennas. *Appl. Phys. Lett.* **2010**, *96*, 211116–211118.
55. Srisungsitthisunti, P.; Ersoy, O. K.; Xu, X. Improving Near-Field Confinement of a Bowtie Aperture Using Surface Plasmon Polaritons. *Appl. Phys. Lett.* **2011**, *98*, 223106–223108.